frontiers | Frontiers in Physics

TYPE Brief Research Report
PUBLISHED 26 January 2023
DOI 10.3389/fphy.2023.1062433

OPEN ACCESS

EDITED BY
Han Zhang,
Institute of Acoustics (CAS), China

REVIEWED BY
Sergey Gurbatov,
Lobachevsky State University of Nizhny Novgorod, Russia
Mohd Ridzuan Ahmad,
University Technology Malaysia, Malaysia

*CORRESPONDENCE
Itziar González,
iciar.gonzalez@csic.es

SPECIALTY SECTION
This article was submitted to Physical Acoustics and Ultrasonics, a section of the journal Frontiers in Physics

RECEIVED 05 October 2022
ACCEPTED 10 January 2023
PUBLISHED 26 January 2023

CITATION
González I, Candil M and Luzuriaga J (2023), Acoustophoretic trapping of particles by bubbles in microfluidics. *Front. Phys.* 11:1062433. doi: 10.3389/fphy.2023.1062433

Acoustophoretic trapping of particles by bubbles in microfluidics

Itziar González[1]*, Manuel Candil[1] and Jon Luzuriaga[1,2]

[1]Laboratory of ultrasonic resonators Result, Institute of Physical technologies and Information ITEFI, Consejo Superior de Investigaciones Científicas CSIC, Madrid, Spain, [2]Signaling Lab, Department of Cell Biology and Histology, Faculty of Medicine and Nursing, University of the Basque Country (UPV/EHU), Leioa, Spain

We present in this paper a simple method to produce strategic acoustic particle capture sites in microfluidic channels in a controlled way. Air bubbles are intermittently injected into a micro-capillary with rectangular cross section during a flow motion of liquid suspensions containing micron-sized particles or particles to create bubble-defined "micro-gaps" with size close to 200 μm and spheroidal geometry. The establishment of a 3D standing acoustic wave inside the capillary at a frequency close to 1 MHz produces different radiation forces on solid particles and bubbles, and acoustic streaming around the bubble. While the sample flows, part of the particles collect along the acoustic pressure node established near the central axis and continue circulating aligned through the capillary until reaching the end, where are released enriched. Meanwhile, the bubble travels very fast toward positions of maximum pressure amplitude beside the channel wall, driven by Bjerkness forces, and attach to it, remaining immovable during the acoustic actuation. Some particles adhere to its membrane trapped by the acoustic streaming generated around the oscillating bubble. Changes of frequency were applied to analyze the influence of this parameter on the bubble dynamics, which shows a complete stability once attached to the channel wall. Only increasing the flow motion induces the bubble displacements. Once reached the open air at the end of the capillary, the bubble disappears releasing the trapped particles separated from their initial host suspension with a purity degree. The device presents a very simple geometry and a low-cost fabrication.

KEYWORDS

microfluidics, acoustofluidics, trapping, particles, bubbles. lab-on-a-chip, acoustic tweezers

1 Introduction

Several applications in microfluidic platforms such as LOC refer to transport samples from one location to another while keeping the sample intact.

Microparticles as well as biological material can be trapped and manipulated in microfluidics using diverse technologies, such as spiral channelizations [1–8], channels including contraction/expansion reservoirs for an alignment of cells, micropillars [9–12],micro-scale vortices [13, 14], micron-sized gaps, serpentine channels or membrane-based microfilters [15–17] with pore diameters. Particles and cells can be handled by ultrasounds, which induce acoustophoretic motions [18–21].

The physics of oscillating bubbles allows diverse applications in microfluidics. An oscillating bubble can act as tweezer for micro-sized objects manipulation, like biological cells. A bubble can be assumed as a soft membrane able to vibrate under the action of external excitation. The response of a bubble can be linear or non-linear depending upon the amplitude of the vibration [22].

Bubbles also can be manipulated in fluids by acoustic fields, named Acoustofluidics: they can be driven toward certain zones of acoustic equilibrium and trapped [23, 24]. The motion of a spherical bubble under the action of a continuously oscillating pressure field can be defined by the Rayleigh–Plesset Eq. 1.

According to classical theory [25], bubbles subject to an acoustic standing wave field gather at either pressure nodes or pressure antinodes depending on whether their fundamental resonance frequencies are below or above the driving frequency. In 1955, Yosioka, Kawasima and Hirano studied the acoustic radiation pressure on bubbles [26]. In 1968, Eller derived an expression for the force experienced by a bubble in a standing acoustic wave. Later, he and Crum studied in 1970 the instability of motion of a pulsating bubble in a sound field [27]. In 1993, Watanabe and Y. Kukita analyzed the translational and radial motions of a bubble in an acoustic standing wave field [28]. They showed that a spherical bubble, not undergoing shape distortions, can also execute irregular translational motions in a standing wave field on the condition that its radial pulsations are vigorous enough.

In microfluidics, acoustic streaming can generate vorticity and then flow mixing with governing viscous forces [29]. But, alternatively, the presence of bubbles in these microfluidic geometries excited at their resonant frequencies can generate intense streaming in the surrounding liquid associated to the vibration induced on the gas/liquid interface of the bubbles [1]. Bubble-around microstreaming is the generation of vortex flows which arise around oscillating ultrasound microbubbles in microfluidics. The vibration of spherical and flattened microfluidic bubbles can produce intense microstreaming when excited by ultrasound near resonance.

In 2007, Manasseh and Ooi [30] confirmed experimentally something observed previously by Marmottant and Hilgenfeldt [31] with nearly spherical bubbles attached to a wall with a finite contact angle: a strong microstreaming for bubbles excited at frequencies near resonance, with vorticity affecting particle trajectories at distances beyond 10 bubble radii. Longuet-Higgins [32] explained in 1998 that intense long-range vorticity results from the combination of two modes of vibration oscillating out of phase. These two modes are in their case the main volume mode and the to-and-fro translation of the bubble centre of mass with respect to the solid surface. This theory completed by Doinikov and Bouakaz [33] in 2010, was developed for freely oscillating spherical bubbles.

Mekki Berrada et al analysed in 2016 the microstreaming flow around an isolated bubble and found a short-range microstreaming around it [34]. To study freely oscillating bubbles in steady conditions, they confined bubbles between the two walls of a silicone microchannel and anchored them on micropits.

Large amplitudes of vibration are obtained when the excitation frequency corresponds to a perimeter that is a multiple of the Faraday wavelength.

Streaming mainly occurs in the bulk due to viscous attenuation. In a second mechanism, observed even in low-dissipation fluids, streaming takes its origin near boundaries where velocity gradients are the strongest and can drive fluid circulations up to the bulk [35]; Holtsmark et al. [36].

These fixed bubbles can be used to trap and deliver a particle or cell to a desired location as acoustic tweezers. But they can promote also formation of stable clusters for a later desired delivery. In the present work, we describe experimental observations of the effects on particles induced by microstreaming developed around and inside semi-flattened bubbles acoustically driven toward a wall of a microfluidic channel by the action of a standing wave.

2 Methods and materials

2.1 Theoretical principle of operation

2.1.1 Radiation force exerted on small particles

Particles or particles in suspension exposed to acoustic waves experience entrainment effects associated to a non-linear interaction between the incident wave and that one scattered by each particle, which generates an acoustic radiation force acting on them. For a particle in a standing wave much smaller than the acoustic wavelength λ, with density ρ_p, compressibility β_p and a volume V_p, this force can be expressed as [37]:

$$F_{Rad} = -\frac{\pi P_0^2 V_p \beta_0}{2\lambda}\varphi(\rho,\beta)\sin(2kx) \tag{1}$$

where $\varphi = \frac{5\rho_p - 2\rho_0}{2\rho_p + \rho_0} - \frac{\beta_p}{\beta_0}$ is the acoustic contrast factor, P_0 the incident wave pressure amplitude, ρ_0 and β_0 the density and compressibility coefficients of the fluid respectively, and "x" the distance from the particle to the nearest node of pressure in the standing wave. According to this equation, the particles collect in parallel bands perpendicular to the sound wave direction, separated by a half wavelength distance (λ/2). The sign of φ indicates the motion of the particles either toward the nodes (φ > 0) or to the antinodes in the standing wave (φ < 0).

The velocity of a particle moving towards a pressure node at distance x from it can be obtained by equating the average ultrasonic force acting to move particles into hands with Stoke's drag force from the quiescent liquid, $F_{Dx} = -6\pi\eta R_p u_{pz}$, neglecting inertial effects for micrometer-sized spherical particles:

$$u_x = \frac{P_0^2 V_p \beta_l}{12\lambda\eta R_p}\varphi\left(\rho_p, \rho_l, \rho\beta_p, \beta_l\right)\sin(2kx) \tag{2}$$

From it, the particle trajectory can be derived as:

$$x(t) = \frac{1}{k}arctan\left\{tan(kx(0))e^{\frac{4\varphi}{3}(kR_p)^2\frac{E_{ac}}{\eta}t}\right\} \tag{3}$$

with the acoustic energy density: $E_{ac} = \frac{p_0^2}{4\rho_0 \cdot c_0^2}$.

We can also calculate the time t it takes a particle to move from any initial position z (0) to any final position z (t):

$$t = \frac{3\eta}{4\Phi(kR_c^2)E_{ac}}ln\left[\frac{tan[k\cdot x(t)]}{tan[k\cdot x(0)]}\right] \tag{4}$$

On the other hand, the shear rate of a liquid sample flowing in a microfluidic channel with rectangular cross-section (width ~ w and depth ~ h) is estimated [38, 39] as:

$$\nu_{shear} = \frac{32Q_{sample}}{\pi d_h^3} = \frac{32(w+h)^3\nu_{flow}}{\pi h^2 w^2} \tag{5}$$

Being s_{sample} the flow rate of the sample $Q_{sample} = \frac{volume}{t} = S\cdot\nu_{flow}$ and d_h the hydraulic diameter of the rectangular channel, defined as $d_h = 2\,wh/(w + h)$. Parabolic profiles are described in Microfluidic flow motion, as shown in Figures 1A, B shows a numerical prediction of acoustophoretic trajectories of three spherical particles derived in Matlab from three different positions in a standing wave while flowing along the channel from left to right (y-axis) in a laminar flow conditions (Stokes regime).

The shear forces are variable within the capillary cross section with the flow parabolic profile, providing a complex contribution to the acoustic radiation force on the particles.

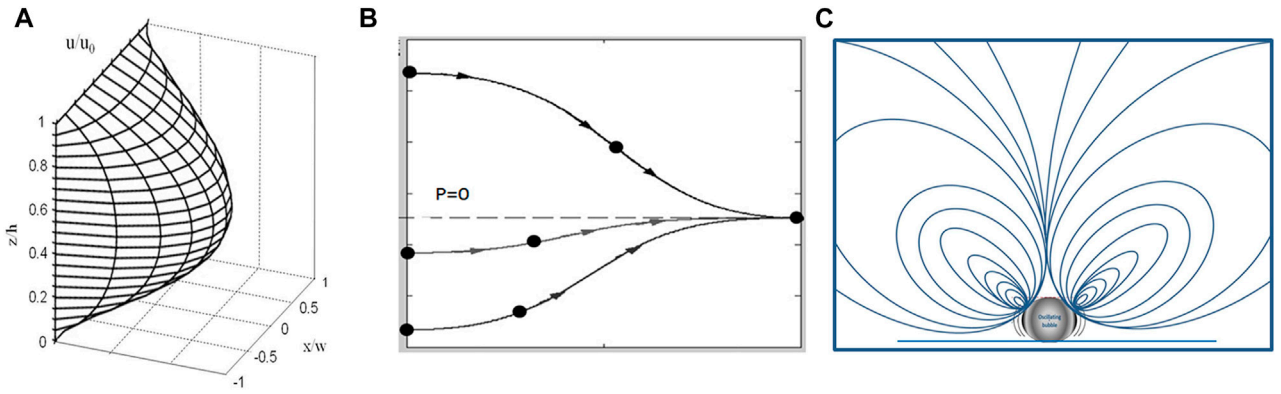

FIGURE 1
(A) parabolic flow motion in a channel of cross section with square geometry; **(B)** numerical simulation of three particles approaching from three initial positions toward the pressure node; **(C)** Schematic of theoretical streamlines generated around an oscillating microbubble.

2.1.2 Motion of a bubble in a standing wave

The equations of motion in the translational and the radial directions are re-derived here using the Lagrangian formalism. A gas bubble undergoes volume and translational oscillations in an ideal incompressible liquid. Using the spherical coordinates (r, θ, ε) originated at the moving center of the bubble, the boundary conditions at the surface of the bubble can be written as

$$\frac{\delta\phi}{\delta r} = \dot{R} + \dot{x}\cos\theta \text{ at r} = \text{R (t)} \tag{6}$$

where ϕ is the velocity potential, R (t) and x (t) are the time dependent radius and position of the center of the bubble, respectively, and the overdot denotes the time derivative [40, 41]. The velocity potential, which must satisfy the Laplace equation.

$\Delta\phi = 0$, can be represented as

$$\phi = \frac{a(t)}{r} + \frac{\dot{b(t)}}{r^2}\cos\theta \tag{7}$$

Substituting Eq. 7 into Eq. 6, we obtain a (t) = $\dot{R}R^2$ and b (t) = $\dot{x}R^3$/2 respectively. The Lagrangian function of the system takes the form:

$$L = 2\rho R^3\left(\dot{R}^2 + \frac{\dot{x}^2}{6}\right) + \frac{4}{3}\pi R^3 p_{sc} + xF_{ex} \tag{8}$$

where p_{sc} is the scattered pressure at the surface of the bubble, $V = 4\pi R^3/3$ is the time-varying volume of the bubble, and F_{ex} refers to external forces on the bubble, such as the primary Bjerknes force or viscous drag.

It is known that a single bubble in a stationary acoustic field is attracted or repulsed at the pressure node or antinode. The force that acts on this single bubble is the primary Bjerknes force [22, 25] is defined as:

$$F_B = -\frac{4\pi R^3 \nabla p_A}{3} \tag{9}$$

where ∇pa represents the gradient of pressure. The kinetic energy T of the system is determined by the kinetic energy of the surrounding liquid [42]. For low amplitude vibrations, a bubble of radius R will resonate at a unique frequency, f, given by [43]:

$$f = \sqrt{\frac{1}{4\rho_l\pi^2R^2}\left[3k\left(P_0 + \frac{2\sigma}{R}\right) - \frac{2\sigma}{R}\right]} \tag{10}$$

where ρ is the density, σ is the surface tension, k is the polytropic exponent of the gas and Po is the hydrostatic pressure and the subscript l denotes liquid. This equation is not applicable for higher amplitudes since the bubbles start to oscillate with harmonics.

A particle moving near a vibrating liquid-gas interface will experience the 'Stokes Drag force' F_{Drag} along the streamline. This force is generated by relative motion between an object and the fluid in which it is immersed [44]:

$$F_{Drag} = 6\pi\eta R_p U_p \tag{11}$$

where η represents the dynamic viscosity, R_p the particle radius and U_p refers to the relative velocity between the particle p and its surrounding fluid. A second-order r-adiation force, known as the Bjerknes force, is generated to act on a particle experiences near an oscillating bubble [22]. It is generated because of a scattering effect of the incoming ultrasonic waves from the liquid–gas interface. This force tends to come out of the center of the bubble and affects the particles that are present within the flow field. It is generally assumed that the particles absorb this scattered radiation acquiring part of the momentum transferred [45].

$$F_{rad} = 4\pi\frac{R_p^3R^4}{d^5}\omega^2\xi^2\left(\frac{\rho_l - \rho_p}{\rho_l + 2\rho_p}\right) \tag{12}$$

where d represents the center-to-center separation between the bubble and the particle; ω denotes the angular frequency and ξ represents the bubble displacement.

According to Eq. 11, the magnitude of the secondary radiation force depends upon the geometries of the particle as well as the amplitude and the frequency at which a bubble is actuated. The sign that determines the direction of the force i.e. whether attractive or repulsive depends on the ratio of the particle and fluid densities. Insonated bubbles are a linear system for low amplitudes at which they exhibit a stable motion: superimposed streamlines are generated around the oscillating microbubble (Figure 1C).

2.1.3 Streaming force generated on a particle by an oscillating bubble in a wave

The adherence of particles on the bubble's membrane is due to the generated acoustic streaming around the bubble. Maramizonouv et al.

presented a study in 2021 [45] to describe acoustic streaming effects on microparticles/droplets in microfluidics. For a laminar flow, the governing equations of the motion in three dimensions (i.e., the continuity and Navier-Stokes equations) can be described as:

$$\frac{\partial U_{ax}}{\partial t} + \nabla \rho_f U_f = 0 \tag{13}$$

$$\frac{\partial \rho_f U_f}{\partial t} + \left(U_f \nabla\right)\rho_f U_f = -\nabla P + \mu_f \nabla^2 U_f + G + F_{AS} \tag{14}$$

where ρ_f is the fluid density, U_f is the fluid velocity vector, t is the time, p is the fluid pressure, μ_f is the fluid viscosity, $G = \rho_f g$ is the gravity force and F_{AS} is the force that the fluid experiences due to the acoustic field (Batchelor, 2000) [46].

For a steady incompressible fluid flow Eqs 13, 14 can be expressed as:

$$\nabla U_f = 0 \tag{15}$$

$$\rho_f\left(U_f \nabla\right)U_f = -\nabla P + \mu_f \nabla^2 U_f + G + F_{AS} \tag{16}$$

The acoustic streaming forces are calculated in a fluid assuming a steady state for both the acoustic and flow fields using a perturbation method (Shiokawa, Matsui and Ueda, 1990) [47]. Thus, the pressure, density and flow field velocity can be described as $P = P_0 + P_a + P_b$, $\rho_f = \rho_0 + \rho_a + \rho_b$ with $\rho_a = P_a/c_f$ [2] and $U_f = U_0 + U_a + U_b$, where 0, a and b indices denote undisturbed state, first order and second order approximations of the three variables pressure p, density ρ and U_f the fluid velocity vector.

The acoustic streaming force, F_{AS}, acts as a body force on the fluid

$$F_{As} = \langle \rho_a \partial t U_a \rangle + \rho_f \langle (U_a \cdot \nabla) U_a \rangle \tag{17}$$

The acoustic streaming force components from Eq. 17 were calculated as:

$$F_{Asx} = \left(\frac{\rho_f}{2} U_{ax}\left(\frac{\partial U_{ax}}{\partial x} + \frac{\partial U_{ay}}{\partial y}\right)\right) + \left(\frac{\rho_f}{2}\left(U_{ax}\frac{\partial U_{ax}}{\partial x} + U_{ay}\frac{\partial U_{ax}}{\partial y}\right)\right) \tag{18}$$

$$F_{Asy} = \left(\frac{\rho_f}{2} U_{ay}\left(\frac{\partial U_{ax}}{\partial x} + \frac{\partial U_{ay}}{\partial y}\right)\right) + \left(\frac{\rho_f}{2}\left(U_{ax}\frac{\partial U_{ay}}{\partial x} + U_{ay}\frac{\partial U_{ay}}{\partial y}\right)\right) \tag{19}$$

where U_{ax} and U_{ay} are the wave velocities in x- and y-directions, respectively.

The acoustic streaming force acts as a body force on the fluid (Ding et al., 2013) [48] and thus Eqs 18, 19 can be substituted as the x and y-components of F_{AS} in Eq. 16.

2.2 Experimental setup and method of operation

The experiments were performed in a glass capillary actuated by a piezoelectric transducer at 1,153 kHz attached to it, hosting 2D orthogonal half-wavelength resonances that generated a single-pressure-node along its central axis where particles collected (Figure 2A). A piezoceramic square ceramic PZ26 (Ferroperm Piezoceramics, Kvistgard, Denmark) of1 dimensions 10 mm × 5 mm × 1 mm was used as acoustic transducer, actuated using a function generator (Agilent 33220A, Agilent Technologies Inc., Santa Clara, CA, United States) equipped with a power amplifier (E&I RF linear broad Amplifier 240 L, Research Blvd. Rochester, NY, United States). The thickness of the piezoelectric ceramic defined a thickness-mode resonance at a frequency close to 1,150 kHz with a half-wavelength standing wave established between the two parallel electrode surfaces.

The channel of the capillary (Vitrocom, Fabrinet company, Mountain Lakes, New Jersey 07,046) had square geometry, with inner dimensions of 700 μm × 700 μm × 5 cm. It allowed the establishment of a half-wavelength resonance within its cross section at a frequency close to 1 MHz, with areas of maximal pressure beside the channel walls and nodal planes interfering along the central axis of the capillary. It was governed by the thickness mode resonance of the piezoelectric actuator. A silicone tubing was coupled to the inlet of the capillary tube for the sample injection. The device was mounted on a microscope slide to aid handling (Figure 3A), placed under a microscope during the acoustic treatment for the sample observation. A Photron CCD camera attached to a Scope A1 Zeiss transmission microscope connected to a computer running a Photron Fastcam Viewer three software were used for the capture, control and processing of the filmed images. A capture speed of the CCD camera of 60 frames/s was selected for the different experiments to achieve clear images of the bubble and particles in motion under the acoustic wave during the flow motion of the sample. The walls of the capillary were made up of Pyrex glass, with a thickness of 145 μm. Intermittent injection of the liquid sample combined with air was performed using a syringe. With this technique, bubbles with radii R0 ranging between 100 μm and 200 μm were obtained and infused together with the liquid sample.

The capillary containing a water-based liquid suspension and exposed to the ultrasounds was modeled and numerically analyzed using the FEM (Finite Element Method) software COMSOL Multiphysics®. Figure 2B shows the 3D acoustic pressure distribution numerically obtained with Comsol Multiphysics inside the channel at a frequency of f = 1153 KHz [49].

3 Results

In the experiments, three simultaneous processes were observed once applied the acoustic field: i) particle collection and alignment along the acoustic pressure node established inside the capillary according to Eq. 1; ii) a very rapid drift motion of the bubble toward the channel wall with a maximal pressure amplitude according to Eq. 9; and iii) adherence of particles to the bubble surface according to Eq. 12 respectively.

First, the solid particles with a positive acoustic contrast factor and size much smaller than the acoustic wavelength experienced the radiation force of Eq. 1 inside the capillary during their flow motion from right to left. They were driven toward the pressure node, established slightly under the central axis along the channel length (see Supplementary Video S1) by the slightly distorted acoustic pressure pattern generated by the presence of the bubble.

Meanwhile, some particles were trapped by the oscillating bubble (one order of magnitude bigger) during and after its drift motion toward the channel wall, where a maximum of pressure amplitude was reached according to Eq. 9; Figure 3A shows a photograph of 100 μm-diameter microbubble taken in the experiments after picking up a single 20 μm polystyrene sphere, which remained adhered to it during the experiments; Figure 3B shows nine particles adhered to the outer surface of a 200 μm-sized spherical bubble by the action of ultrasounds during a flow motion under laminar flow motion regime exposed to a quasi-standing wave. The particles were entrained and dragged by the streamlines created around the oscillating bubble to adhere to its surface

10.3389/fphy.2023.1062433

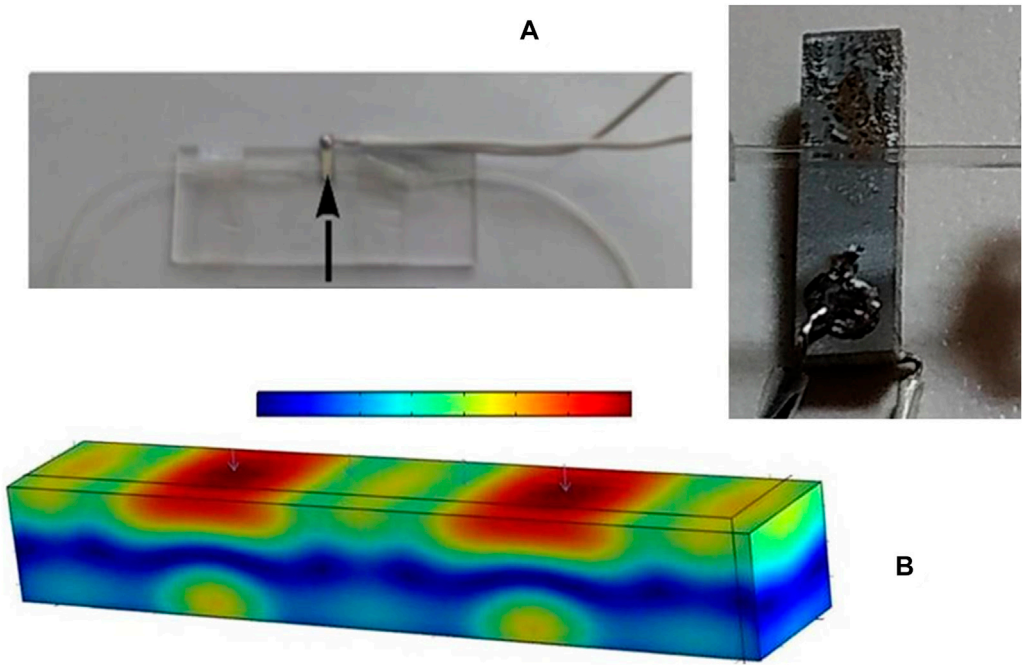

FIGURE 2
(A) Experimental setup including the microfluidic capillary and a piezoelectric transducer attached underneath; **(B)** 3D acoustic pressure distribution numerically obtained with Comsol Multiphysics inside the channel at a frequency of f = 1153 KHz containing water-based liquid samples [49].

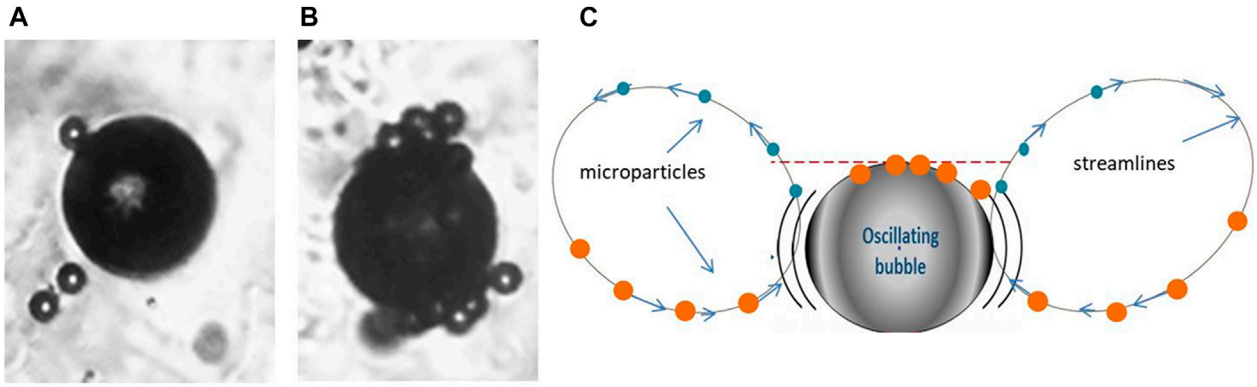

FIGURE 3
(A) photographs of a microbubble (ϕ = 100 μm) with a single 20 μm glass sphere adhered to it and; **(B)** ten particles adhered to the outer surface of a 200 μm-sized spherical bubble by the action of ultrasounds; **(C)** scheme of the particle adherence process onto the oscillating bubble due to the acoustic streaming generated around it.

(Figure 3C), according to the microstreaming pattern generated by oscillating bubbles in bulk fluid [32]. When particles reach the membrane of the bubble they are trapped in it.

On the other hand, the bubble, with a diameter approximately 10 times larger than those of the particles (20 μm), is rapidly driven and trapped in a position beside the wall where the acoustic pressure acquires maximal amplitude. Bubbles in a standing wave are exposed to Bjerkness forces and are rapidly driven toward these locations of acoustic equilibrium.

It is known that the direction of the radiation force depends on the ratio between the frequency of the external force and the resonant frequency of the bubble. According to theory [22, 25], small bubbles compared to the resonant frequency (which is inversely proportional to the bubble radius: f [kHz] ~ 3/R [mm]) are drawn into the strong field region, while large ones are pushed out into the weak field region. However, in the current experiment, a rather large bubble (~100 μm) at a field frequency of about 1 MHz is pushed towards the wall, where the field antinode seems to be.

A Supplementary Video S1 (Video1.mp4) shows this behaviour. Once the air-filled sphere was attached to the solid-wall remained fixed during the whole experiment. Bubble oscillations could not be distinguished from the filmed images because the temporal resolution

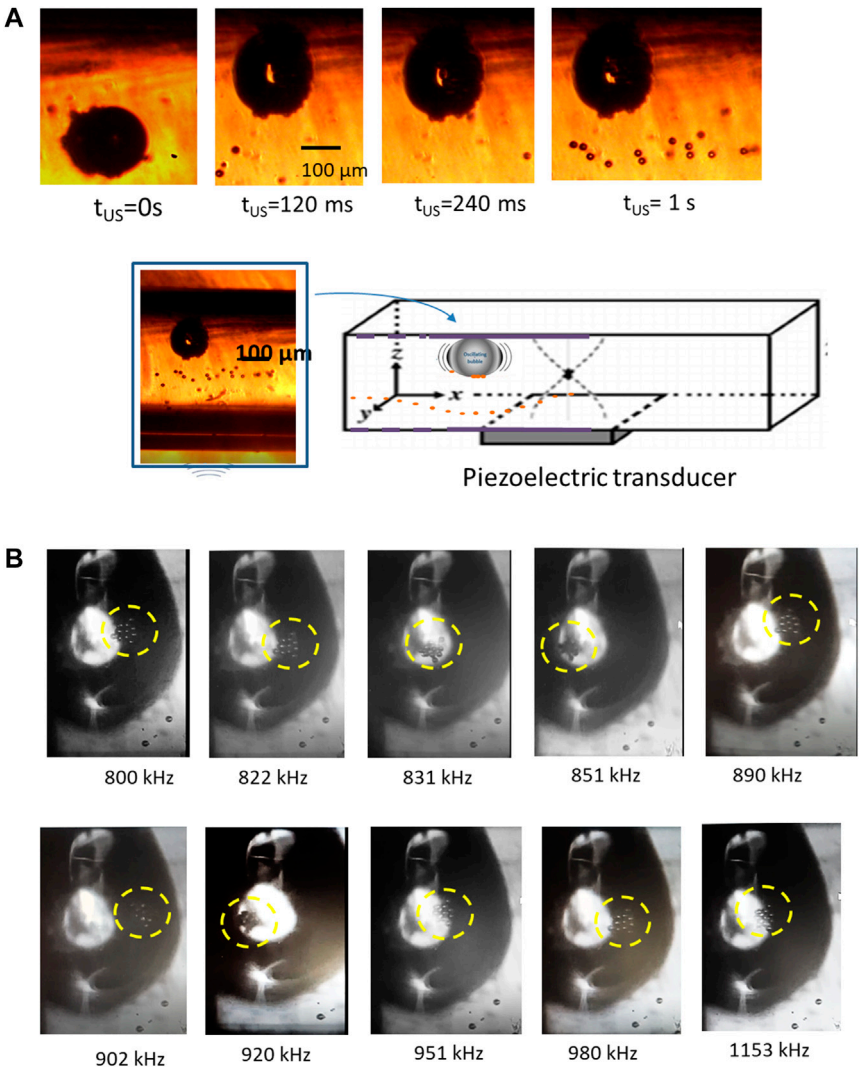

FIGURE 4
Different times filmed on the bubble with polystyrene particles; **(A)** the bubble was acoustically trapped on the wall in less than 120 ms and remained immovable all the time during the acoustic actuation; **(B)** different positions of the polystyrene bead aggregate apparently found on the bubble surface at different acoustic frequencies ranging from 800 kHz up to 1,200 kHz.

associated to the CCD capture speed is various orders of magnitude lower than the acoustic periods tested.

The drift motion of the polystyrene small particles toward the pressure node was slower, as shown in subsequent photos of Figure 4A: it took a time close to 1 s against the 34 ms approximately required by the bubble to reach the channel wall.

The particles trapped by the bubble remained attached to its membrane and formed a cluster that described certain displacements and rotations on the bubble surface when it was exposed to different acoustic conditions.

During the experiments, the frequency of the acoustic wave was varied within a range varying from 800 kHz up to 1,200 kHz to analyze the stability of the oscillating bubble once adhered to the channel wall. The frequency variations produce relevant variations in the spatial 3D acoustic pressure pattern inside the capillary. In consequence, displacements of the bubble should be expected.

Figure 4B shows ten captured images of the bubble with a cluster of particles adhered to its surface exposed to the ultrasonic wave at different frequencies ranging from 800 kHz up to 1,200 kHz.

The cluster shows different positions on the bubble at each frequency. Comparing the images of the figure, identical positioning of the cluster was found at f = 980 kHz and 820 kHz respectively (Δf = 160 kHz). This can mean either a complete rotation of 360° with the frequency variation of 180 kHz, or an oscillatory partial rotation of the bubble toward first one sense followed by a an opposite direction half-rotation. In consequence, the particle aggregate appears in the same position at both frequencies. It can not be distinguished from the images of the experiments which of both possible motions happened from the experiments at the capture speed of the camera.

On the other hand, the particle aggregate presents similar positions on the bubble surface at frequencies of 1153 kHz and 951 kHz, which corresponds to a frequency variation Δf = 202 kHz. Frequencies of 890 kHz and 800 kHz provide also similar positions for the cluster on the bubble (Δf = 90 kHz), as well as similar patterns were found at 920 kHz and 851 kHz respectively. In this case, the particle aggregate seem to be behind the bubble, which means an abrupt horizontal rotation of almost 270° (or alternatively 90°) in a frequency

rise of approximately 70 kHz. Finally, the cluster was found just centered with the bubble at the frequency of 831 kHz.

Intermediate frequencies between these described above did not provide clear changes in the particle positions over the bubble surface.

4 Discussion

First, the amplitude of the acoustic pressure established inside the channel was low enough, so that the variations of frequency did not generate deformations in the shape of the bubble, but instead they induced either rotations of the bubble around its centre of gravity or coherent displacements of the particles trapped on its surface.

The experiments revealed the stability of the bubble once adhered to the channel wall. Neither displacements nor landslides were found along such a surface despite the strong variations of the spatial pressure changes associated to the frequency variations.

On the other hand, no rotational movement of the bubble has been directly evidenced with the frequency variations. However, the particles adhered to its surface showed either displacements on the bubble surface, or, if it was not the case, they would be indicators of the bubble rotation. This could not be elucidated in our experiments.

Anyway, the different positions found on the particle cluster position over the bubble surface do not show a linear correlation with the frequency variations, which could be due to the abrupt changes of the pressure pattern induced inside the capillary.

Finally, it should be remarked the absence of displacement of the bubble in the face of any change in frequency tested. The bubble remains stable attached to the upper wall of the channel without experiencing slippage on it at any of the frequencies tested. This translational motion could be only achieved only by increasing the flow rate of the sample circulating along the capillary. This was the way to transport the bubble with the particle aggregate adhered until the end of the channel, where collapsed releasing the particles previously trapped separately from their initial host sample.

5 Conclusion

An oscillating bubble can act as tweezer for micro-sized objects manipulation, like biological cells. In particular, the experiments of the current paper have shown the ability of a bubble in microfluidics to trap small particles and drive them toward places of acoustic equilibrium that not correspond to those initially predicted for them. The secondary radiation force generated by the bubble can be used to capture the particles, and flow motion can be used to move the bubble to a desired location for particle release. A competition between the radiation force and the drag force allows this transport. The microbubbles have shown to be remarkably resilient to certain variations of the acoustic field conditions.

This novel mechanism of using a single bubble for micro manipulation could be promising in acoustophoretic processes. It relies on a non-contact based approach of the bubble tweezer to manipulate micro-objects *via* action-at-a-distance principle.

Acoustic oscillating microbubbles have shown a huge potential for numerous applications that could be easily incorporated into existing microfluidic platforms to achieve various tasks. Our experiments confirm that acoustically actuated microbubbles are a suitable agent for transporting matter. Our objective in this experimental study was to know the ability of oscillating bubbles to manipulate smaller particles in a flowing sample under the action of ultrasounds. Streamlines of the secondary flow are linear and parallel to the wall on which a bubble is attached, rather than vertical.

Data availability statement

The original contributions presented in the study are included in the article/Supplementary Material, further inquiries can be directed to the corresponding author.

Author contributions

The corresponding IG provided the idea of this research and participated in the experiments and writing process. JL developed majority of the experiments and contributed to the writing process. Author MC contributed to perform the experiments.

Funding

This work is financed by the Spanish National Plan project PID2021-128985OB-I00 funded by the Spanish Ministery of Science and Innovation MICINN and CSIC-Intramural project.

Acknowledgments

The authors want to acknowledge the support of the Spanish Ministry of Science and Innovation.

Conflict of interest

The authors declare that the research was conducted in the absence of any commercial or financial relationships that could be construed as a potential conflict of interest.

Publisher's note

Supplementary material

The Supplementary Material for this article can be found online at: https://www.frontiersin.org/articles/10.3389/fphy.2023.1062433/full#supplementary-material

References

1. Gossett DR, Weaver WM, Mach AJ, Hur SC, Kwong Tse HT, Lee W, et al. Label-free cell separation and sorting in microfluidic systems. *Anal Bioanal Chem* (2010) 397: 3249–67. doi:10.1007/s00216-010-3721-9

2. Yamada M, Seki M. Hydrodynamic filtration for on-chip particle concentration and classification utilizing microfluidics. *Lab Chip* (2005) 5:1233–9. doi:10.1039/b509386d

3. Yi C, Li C, Ji S, Yang M. Microfluidics technology for manipulation and analysis of biological cells. *Anal Chim Acta* (2006) 560:1–23. doi:10.1016/j.aca.2005.12.037

4. Pamme N. Continuous flow separations in microfluidic devices. *Lab Chip* (2007) 7: 1644–59. doi:10.1039/b712784g

5. Bhagat AA, Bow H, Wei Hou H, Tan SJ, Han J, Lim CT. Microfluidics for cell separation. *Med Biol Eng Comput* (2010) 48:999–1014. doi:10.1007/s11517-010-0611-4

6. Hou HW, Warkiani ME, Khoo BL, Li ZR, Soo RA, Tan DS, et al. Isolation and retrieval of circulating tumor cells using centrifugal forces. *Sci Rep* (2013) 3:1259. doi:10.1038/srep01259

7. Warkiani ME, Guan G, Luan KB, Lee WC, Bhagat AA, Chaudhuri PK, et al. Slanted spiral microfluidics for the ultra-fast, label-free isolation of circulating tumor cells. *Lab Chip* (2014) 14(1):128–37. doi:10.1039/c3lc50617g

8. KhooWarkiani BLME, Tan DS, Bhagat AA, Irwin D, LauLim DPAS, Lim KH, et al. Clinical validation of an ultra high-throughput spiral microfluidics for the detection and enrichment of viable circulating tumor cells. *PLoS One* (2014) 9(7):e99409. doi:10.1371/journal.pone.0099409

9. Nagrath S, Sequist LV, Maheswaran S, Bell DW, Irimia D, Ulkus L, et al. Isolation of rare circulating tumour cells in cancer patients by microchip technology. *Nature* (2007) 450(7173):1235–9. doi:10.1038/nature06385

10. Bhagat AAS, Hou HW, Li LD, Lim CT. Pinched flow coupled shear-modulated inertial microfluidics for high-throughput rare blood cell separation. *J Han, Lab A Chip* (2011) 11:1870–8. doi:10.1039/c0lc00633e

11. Sarioglu F, Aceto N, Kojic N, Donaldson MC, Zeinali M, Hamza B, et al. A microfluidic device for label-free, physical capture of circulating tumor cell clusters. *Nat Methods* (2015) 12(7):685–91. doi:10.1038/nmeth.3404

12. Kim B, Lee JK, Choi S. Continuous sorting and washing of cancer cells from blood cells by hydrophoresis. *Biochip J* (2016) 10(2):81–7. doi:10.1007/s13206-016-0201-0

13. Huang LR, Cox EC, Austin RTH, Sturm C. Continuous particle separation through deterministic lateral displacement. *Science* (2004) 304:987–90. doi:10.1126/science.1094567

14. CheYu JV, Dhar M, Renier C, Matsumoto M, HeirichGaron KEB, Goldman J, et al. Classification of large circulating tumor cells isolated with ultra-high throughput microfluidic Vortex technology. *Oncotarget* (2016) 7(11):12748–60. doi:10.18632/oncotarget.7220

15. Tan SJ, Lakshmi RL, Chen PF, Lim WT, Yobas L, Lim CT. Versatile label free biochip for the detection of circulating tumor cells from peripheral blood in cancer patients. *Biosens &Bioelectronics* (2010) 26:1701–5. doi:10.1016/j.bios.2010.07.054

16. Kuo JS, Zhao YX, Schiro PG, Ng LY, Lim DSW, Shelby JP, et al. Deformability considerations in filtration of biological cells. *Lab A Chip* (2010) 10:837–42. doi:10.1039/b922301k

17. Dessitter I, Guerrouahena BS, Benali-Furet N, Weschler J, Janne PA, Kuang Y, et al. A New device for rapid isolation by size and characterization of rare circulating tumor cells. *Anticancer Res* (2011) 31:427–42.

18. Haake A, Neild A, Kim D, Ihm J, Sun Y, Dual J, et al. Manipulation of cells using an ultrasonic pressure field. *Ultrasound Med Biol* (2005) 31:857–64. doi:10.1016/j.ultrasmedbio.2005.03.004

19. Kapishnikov S, Kantsler V, Steinberg V. Continuous particle size separation and size sorting using ultrasound in a Microchannel. *J Stat Mech Theor Exp.* (2006) 2006:P01012. doi:10.1088/1742-5468/2006/01/p01012

20. Laurell T, Petersson F, Nilsson A. Chip integrated strategies for acoustic separation and manipulation of cells and particles. *Chem Soc Rev* (2007) 36:492–506. doi:10.1039/b601326k

21. González I, Fernandez LJ, Gomez T, Berganzo J, Soto JL, Carrato A. A polymeric chip for micromanipulation and particle sorting by ultrasounds based on a multilayer configuration. *Sens Actuators B Chem* (2010) 144:310–7. doi:10.1016/j.snb.2009.10.042

22. Leighton T. *The acoustic bubble*. San Diego: Academic Press (1994).

23. Hawkes J, Coakley WT. Force field particle filter combining ultrasound standing waves and laminar flow. *Sens Actuators B Chem* (2001) 75:213–22. doi:10.1016/s0925-4005(01)00553-6

24. Doinikov A, Bouakaz A. Acoustic microstreaming around a gas bubble. *J Acoust Soc Am* (2010) 127(2):703–9. doi:10.1121/1.3279793

25. Eller A. 'Force on a bubble in a standing acoustic wave. *J Acoust Soc Am* (1968) 43: 170–1. doi:10.1121/1.1910755

26. Yosioka K, Kawasima Y, Hirano H. 'Acoustic radiation pressure on bubbles and their logarithmic decrement. *Acustica* (1955) 5:173.

27. Eller A, Crum LA. 'Instability of the motion of a pulsating bubble in a sound field. *J Acoust Soc Am* (1970) 47:762–7. doi:10.1121/1.1911956

28. Watanabe T, Kukita Y. 'Translational and radial motions of a bubble in an acoustic standing wave field. *Phys Fluidsa* (1993) 5:2682–8. doi:10.1063/1.858731

29. Lei J, Hill M, Glynne-Jones P. Numerical simulation of 3D boundary-driven acoustic streaming in microfluidic devices. *Lab Chip* (2014) 14(3):532–41. doi:10.1039/C3LC50985K

30. Tho P, Manasseh R, Ooi A. Cavitation microstreaming patterns in single and multiple bubble systems. *J Fluid Mech* (2007) 576:191–233. doi:10.1017/S0022112006004393

31. Marmottant P, Hilgenfeldt S. Controlled vesicle deformation and lysis by single oscillating bubbles. *Nature* (2003) 423(6936):153–6. doi:10.1038/nature01613

32. Longuet–Higgins MS, Particle drift near an oscillating bubble, Proceedings of the Royal Society of London. Series A: Mathematical, Physical and Engineering Sciences.(1998). doi:10.1098/rspa.1997.0083

33. Doinikov AA, Bouakaz A. Acoustic microstreaming around an encapsulated particle. *J Acoust Soc Am* (2010) 127(3):1218–27. doi:10.1121/1.3290997

34. Mekki-Berrada F, Combriat T, Thibault P, Marmottant P. Interactions enhance the acoustic streaming around flattened microfluidic bubbles. *J Fluid Mech* (2016) 797:851–73. doi:10.1017/jfm.2016.289

35. Westervelt PJ. The theory of steady rotational flow generated by a sound field. *The J Acoust Soc America* (1953) 25(60):60–7. doi:10.1121/1.1907009

36. Holtsmark J, Johnsen I, Sikkeland T, Skavlem S. Boundary layer flow near a cylindrical obstacle in an oscillating incompressible fluid. *J Acoust Soc America* (1954) 26:102. doi:10.1121/1.1907271

37. Gor'kov LP. On the forces acting on a small particle in an acoustical field in an ideal fluid. *Sov Phys Dokl* (1962) 6:773–5.

38. Zheng X, Silber-Li Z. Measurement of velocity profiles in a rectangular microchannel with aspect ratio α = 0.35. *Experiments in Fluids* (2008) 44:951–9. doi:10.1007/s00348-007-0454-4

39. Kashaninejad NA. New form of velocity distribution in rectangular microchannels with finite aspect ratios. *Preprints* (2019) 2019:2019050316. doi:10.20944/preprints201905.0316.v1

40. Tokmakov PE, Gurbatov SN, Didenkulov IN, Pronchatov-Rubtsov NV. On influence of an acoustic field on spatial distribution of gas bubbles in a resonator. *Vestnik Nizhny Novgorod State Univ Radiophysics* (2006) 1(4):31–40.

41. Didenkulov IN, Korchagina TS, Pronchatov-Rubtsov NV, Sagacheva AA. Propagation of sound in suspensions: Rotational motions of particles and controlling flows. *Bull Russ Acad Sci Phys* (2020) 84:634–7. No.6. doi:10.3103/s1062873820060076

42. Doinikov A. Translational motion of a spherical bubble in an acoustic standing wave of high intensity. *Phys Fluids* (2002) 14(4):1420–5. doi:10.1063/1.1458597

43. Crowe CT, Schwarzkopf JD, Sommerfeld M, Tsuji Y. *Multiphase flows with droplets and particles*. United States: CRC Press (2012).

44. Brennen CE. *Cavitation and bubble dynamics*. United Kingdom: Oxford University Press (1995).

45. Maramizonouz S, Rahmati M, Link A, Franke T, Fu Y. Numerical and experimental studies of acoustic streaming effects on microparticles/droplets in microchannel flow. *Int J Eng Sci* (2021) 169:103563. doi:10.1016/j.ijengsci.2021.103563

46. Batchelor GK. *An Introduction to fluid dynamics*. Cambridge: Cambridge Mathematical Library)Cambridge University Press (2000).

47. Shiokawa S, Matsui Y, Ueda T. Study on SAW streaming and its application to fluid devices. *Jpn J Appl Phys* (1990) 29(S1):137. doi:10.7567/jjaps.29s1.137

48. Ding X, Li P, Lin SCS, Stratton ZS, Nama N, Guo F, et al. Surface acoustic wave microfluidics. *Lab A Chip* (2013) 13(18):3626–49. doi:10.1039/c3lc50361e

49. de los Reyes E, Acosta V, Carreras P, Pinto A, Gonzalez I. Three-dimensional numerical analysis as a tool for optimization of acoustophoretic separation in polymeric chips. *J Acoust Soc America* (2021) 150:646–56. doi:10.1121/10.0005629